Journal of Molecular Structure 1266 (2022) 133378

Contents lists available at ScienceDirect

Journal of Molecular Structure

journal homepage: www.elsevier.com/locate/molstr

Persistent prevalence of non-covalent interaction in pyrimidine containing sulfonamide derivative: A quantum computational analysis

T.N. Lohith[a], M.K. Hema[a], C.S. Karthik[b,*], S. Sandeep[b], L. Mallesha[c,*], Norah Salem Alsaiari[d], M.A. Sridhar[a], Khadijah M. Katubi[d], Khamael M. Abualnaja[e], N.K. Lokanath[a], P. Mallu[b], S.R. Kumaraswamy[f]

[a] Department of Studies in Physics, Manasagangotri, University of Mysore, Mysuru, Karnataka 570 006, India
[b] Department of Chemistry, SJCE, JSS Science and Technology University, Mysuru, Karnataka 570 006, India
[c] PG Department of Studies in Chemistry, JSS College of Arts, Commerce and Science, Ooty Road 25, Mysuru, India
[d] Department of Chemistry, College of Science, Princess Nourah bint Abdulrahman University, P. O. Box 84428, Riyadh 11671, Saudi Arabia
[e] Department of Chemistry, College of Science, Taif University, Taif 21944, Saudi Arabia
[f] Department of Physics, Maharani's College, Mysuru, Karnataka 570005, India

ARTICLE INFO

Article history:
Received 5 November 2021
Revised 14 May 2022
Accepted 24 May 2022
Available online 26 May 2022

Keywords:
Pyrimidine
Sulfonamide
Single crystal X-ray diffraction and DFT

ABSTRACT

A novel pyrimidine containing sulfonamide derivative has been synthesized and characterized by spectroscopic techniques like FT-IR, NMR and Mass. Single crystal X-ray diffraction study revealed that the title molecule is crystallized in the triclinic crystal system with the *P-1* space group. Structural investigation inferred that the crystal packing is mainly stabilized by N–H…O and C–H…O intermolecular interactions, also by weak C–H…π and C-X…π [*X*=Br, Cl] interactions. Further, Hirshfeld surface analysis was employed to explore the noncovalent interactions which are responsible for the crystal packing quantitatively. In addition, quantum chemical calculations have been performed to validate the non-covalent interactions present in the title molecule. The molecular geometry of the compound is optimized at the DFT/WB97XD/6-311G(d,p) level of theory. The NBO analysis was carried out to know the intramolecular charge transfer in the molecule. Finally, the thermodynamic properties of the title compound have been calculated at different temperatures.

1. Introduction

In recent years, the non-covalent interactions (NCIs) have been the focus of intense investigation in chemistry due to their key role in several fields of science and technology, such as biology, nanotechnology, or materials chemistry [1]. NCIs are key components in the dynamics of life; examples can be including the functioning of DNA and proteins, the mechanisms of medications structure, and properties of chemical structure [2,3]. Designing new solid-state materials with desirable features, such as effective biological activity, is gaining more interest. The primary factors that determine the bioactivity of active chemical substances are solubility, stability, and bioavailability. Crystal engineering is the study of how non–covalent interactions can be used to create new crystalline networks with desired physicochemical properties of chemical compounds [4–6]. Physicochemical properties such as pharmacological activity are induced by the molecular crystal structures of different polymorphs with varying arrangements [7].

The wide variety of applications of pyrimidine derivatives make them one of the important heterocyclic compounds [8]. The pyrimidine derivatives are also have been found to exhibit a wide range of pharmacological activities, such as anti-bacterial [9], anti-inflammatory [10], anti-cancer [11] The study of their geometry, physical and electronic properties has become an interesting field in the research of drug design. Sulfonamides have great synthetic and medicinal importance because of their ability to act as precursors for the synthesis of a variety of biologically important heterocyclic compounds and also inhibits the growth of bacteria due to presence of NH and SO_2 group of sulfonamides [12]. Substituted pyrimidines are already well established as key cores in medicinal chemistry, along with that the sulfonamides have lot of biological significance [13]. Synthesis of sulfa drugs required harsh reaction conditions, hazardous and polluting chlorinating agents or oxidants [14]. To overcome these problems, a lead-free catalyzed reaction has been evolved to treat many infectious diseases. Many sulfonamides derivatives show an excellent non-linear optical (NLO) property [15]. Multifunctional ligands with O–, N–, and

* Corresponding authors.
E-mail addresses: csk@jssstuniv.in (C.S. Karthik), mallesha83@gmail.com (L. Mallesha).

https://doi.org/10.1016/j.molstruc.2022.133378
0022-2860/

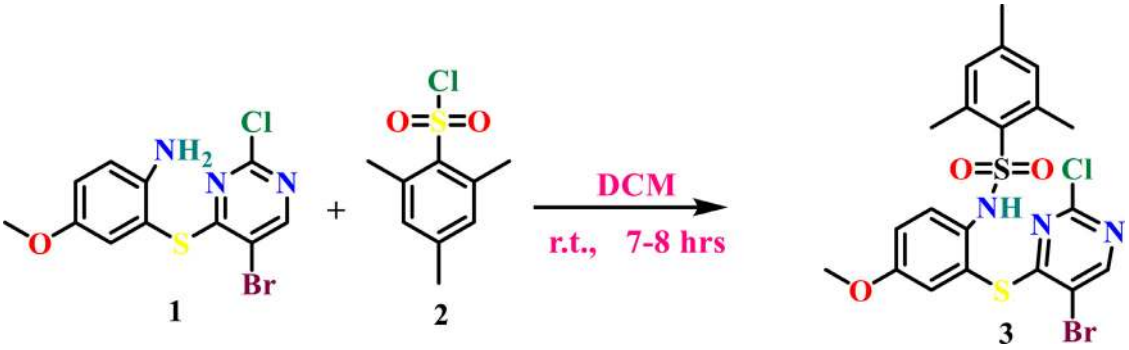

Scheme 1. Synthetic rote for compound **3**.

S–donor atoms can construct and expand linked supramolecular frameworks throughout diverse dimensionality scales for various applications [16–19]. Controlling non–covalent interactions such as Hydrogen Bonds (HBs), Halogen Bonds, and $\pi\cdots$Stacking Forces should be used for self–assembly and the formation of the desired functional compounds [20,21]. Inforecite of the above discussion, pyrimidine coupled sulfonamide derivative was crystallized, and structure was elucidated using SXRD. The noncovalent interactions were investigated in the present work.

2. Materials and methods

All solvents and reagents were purchased from Merck chemicals. Melting range was determined by Veego Melting Point VMP III apparatus. Elemental analyses were recorded on VarioMICRO superuser V1.3.2 Elementar. The FT-IR spectra were recorded using KBr discs on FT-IR Jasco 4100infrared spectrophotometer.1H NMR spectra were recorded on Bruker DRX −500 spectrometer at 400 MHz usingd6-DMSO as solvent and TMS as internal standard. Silica gel column chromatography was performed using Merck7734 silica gel (60–120 mesh) and Merck-made TLC plates.

2.1. Synthesis of N-[2-(5–bromo-2–chloro-pyrimidin-4-ylsulfanyl)−4–methoxy-phenyl]−2,4,6-trimethyl-benzenesulfonamide (3)

The experimental procedure described as per our previous research [22] afforded 3, and the product obtained from 2-(5–bromo-2-chloropyrim-idin-4-ylthio)−4-methoxybenzenamine (1) (3.47 g, 0.01 mol) and 2,4,6-trimethylbenzene-1-sulfonyl chloride (2) (2.19 g,0.01 mol) as shown in Scheme 1. The compound 3 is dissolved in ethanol and kept for slow evaporation at ambident temperature for 4 days. FT-IR (KBr, cm1)m: 3176 (N–H), 2924 (C–H),1698 (C,N), 1463 (C,C), 1376 (C–N), 1151 (C–O), 722(C–Cl), 521 (C–Br).1H NMR (DMSO–d6, 400 MHz)d: 9.66(s, 1H, Pyrimidine-H), 8.55 (s, 1H, Ar-H), 7.47 (d, 1H, Ar-H), 7.14 (d, 1H, Ar-H), 7.03 (s, 1H, NH), 6.61 (s, 2H, Ar-H), 3.71 (s, 3H, OCH3), 2.29–1.99 (s, 9H, CH3). MS (ESI)*m/z*: 529.0. Anal. calcd. for C20H19BrClN3O3S2(in%): C-45.42, H-3.62, N-7.95. Found C-45.62, H-3.72, N-8.12.

2.2. Single crystal X-ray crystallography

A white colored single crystal with approximate dimensions 0.25 mm ✗ 0.22 mm ✗ 0.18 mm was selected for the X-ray diffraction study. The X-ray intensity data were collected on a Bruker Kappa Apex-II diffractometer having an X-rays tube containing molybdenum as a target. The graphite monochromator and CCD were used for recording the intensity peaks. APEX-II and SAINT software were used to carry-out for data collection and data reduction [23]. SHELXS97 was employed for structure solution [24] and SHELXL2018/3 was used for the structure refinement [25]. Anisotropic refinement was done for all the non-hydrogen atoms. A total of 325 parameters were refined with 16,395 unique reflections. The final residual factor, *R* converged to 0.0649 and the goodness of fit was 1.039. The standard geometrical calculations were done using the program PLATON [26] and the thermal ellipsoidal plot was generated using the software Mercury4.0 [27].

2.3. Quantum computational details

The complete quantum chemical computations of the title compound *N* -[2-[(5-Bromo-2–chloro-4-pyrimidinyl)thio]−4-methoxyphenyl]−2,4,6-trimethylbenzenesulfonamide were performed with the help of the Gaussian09 package [28]. The explicit dispersion correction incorporated in the computational methodology improves the accuracy of the results by accounting for van der Waals interactions and is essential for agreement with experimental data. The entitled compound was optimized using single crystal X-ray diffraction based geometries at the DFT/WB97XD/6–311G(d,p) level [29]. Further, the ground state energy, FMO analysis, and global reactive parameters were assessed by using the optimized structure. The optimized and 3D molecular orbitals were visualized by using the software GaussView 6.0 [30]. The Natural Bond Orbital (NBO) calculations were carried out using the aforesaid level of theory. Also, the knowledge of the reactive sites present in the molecule was obtained by the analysis of molecular electrostatic potential (MEP) [31]. In addition, quantum theory of atoms in molecules (QTAIM) analysis was also carried out to unravel the electron density $\rho(r)$ values at the bond critical points (BCPs) established between each atom of the title molecule. The non-covalent interaction (NCI) analysis was also done to explore the weak interactions present in the title molecule. The AIM and NCI calculations were performed using Multiwfn 3.7 package [32] and the results were visualized by using Visual Molecular Dynamics (VMD) software [33]. In addition, the aforesaid method was also used to compute certain thermodynamic properties viz., zero-point vibrational energy (ZPVE) (kcal mol^{-1}), rotational constants (GHz), heat capacity at constant volume (C_v) (cal $mol^{-1}K^{-1}$), heat capacity at constant pressure (C_p) (cal mol^{-1} K^{-1}), entropy (S) (cal $mol^{-1}K^{-1}$), enthalpy change ($\Delta H_{0\rightarrow T}$) (kcal mol^{-1}), dipole moment μ (Debye) [34].

3. Results and discussion

3.1. X-ray crystal structure analysis

Molecular structure of *N*-[2-[(5–bromo-2–chloro-4-pyrimidinyl)thio]−4-methoxyphenyl]−2,4,6-trimethyl benzene sulfonamide, is confirmed by the single crystal X-ray diffraction analysis and crystallizes in the triclinic space group $P\bar{1}$. The *ORTEP* diagram is depicted in Fig. 1. Summary of the crystal structure

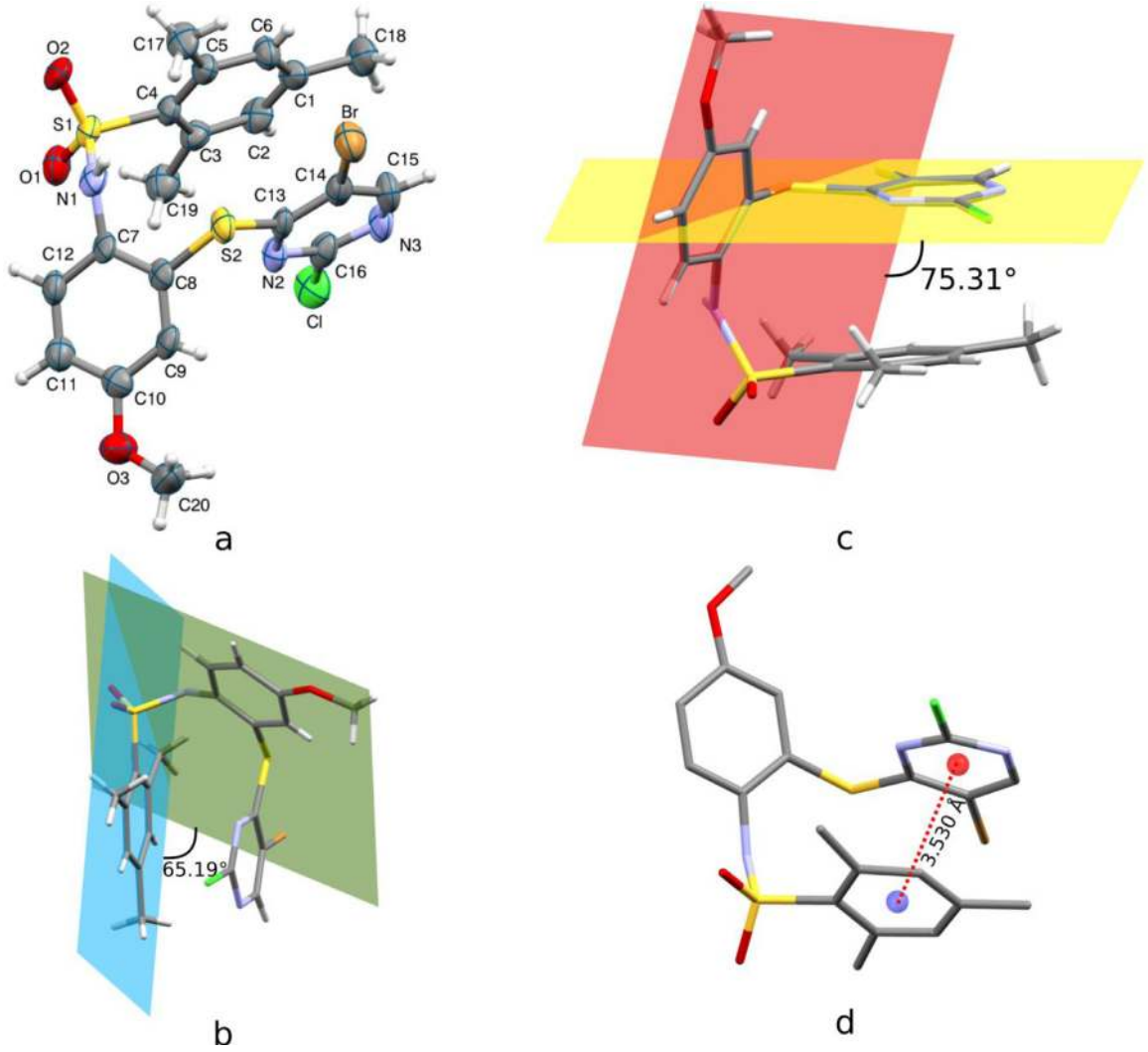

Fig. 1. (a) *ORTEP* with atom numbering scheme where thermal ellipsoids drawn at 50% probability, (b and c) planarity representation and (c) intramolecular $\pi \ldots \pi$ stacking between trimethyl and chloro–bromo substituted pyrimidinyl rings of benzene sulfonamide crystal structure.

data and refinement details are listed in Tables 1a and 1b. The selected values of bond lengths, bond angles, and torsion angles

Table 1a
Crystal data and structure refinement details of the title compound.

Parameter	Value
CCDC number	2,115,842
Empirical formula	$C_{20}H_{18}BrClN_3O_3S_2$
Formula weight	528.87
Temperature	300 K
Wavelength	0.71073 Å
θ range	1.48°–25.00°
Crystal system	Triclinic
Space group	$P\bar{1}$
Cell parameters	a = 8.046(3) Å
	b = 9.910(2) Å
	c = 14.640(7) Å
	α = 99.511(14)°
	β = 93.942 °
	γ = 101.639(14)°
Volume	1074.1(8) Å^3
Z	2
Density (calculated)	1.635 Mg m^{-3}
Absorption coefficient	2.261 mm^{-1}

(*continued on next page*)

Table 1a (*continued*)

Parameter	Value
F_{000}	536
Crystal size	0.20 mm ✗ 0.15 mm ✗ 0.10 mm
Index ranges	$-9 \le h \le 9$
	$-11 \le k \le 11$
	$-17 \le l \le 17$
Reflections collected	16,395
Independent reflections	3772 [R_{int} = 0.0990]
Absorption correction	Multi-scan
Refinement method	Full matrix least-squares on F^2
Data/restraints/parameters	3773/0/325
Goodness-of-fit	1.039
Final [$I > 2\sigma(I)$]	R_1 = 0.0649, wR_2 = 0.1622
R indices (all data)	R_1 = 0.1028, wR_2 = 0.1838
Largest diff. peak and hole	0.586 and –0.909 e Å^{-3}

Table 1b
Intramolecular and Intermolecular hydrogen bond geometry of the title molecule.

D-H…A	D-H (Å)	H…A (Å)	D…A (Å)	D-H…A (Å)
N1-H1N…O2^i	0.72	2.42	3.038 (8)	146 (8)
C17-H17B…O2^a	0.87	2.59	2.890 (10)	101 (6)
C18-H18A…O2^{ii}	0.96	2.40	3.343 (8)	167
C19-H19B…O1^a	0.87	2.36	2.726 (10)	106 (5)

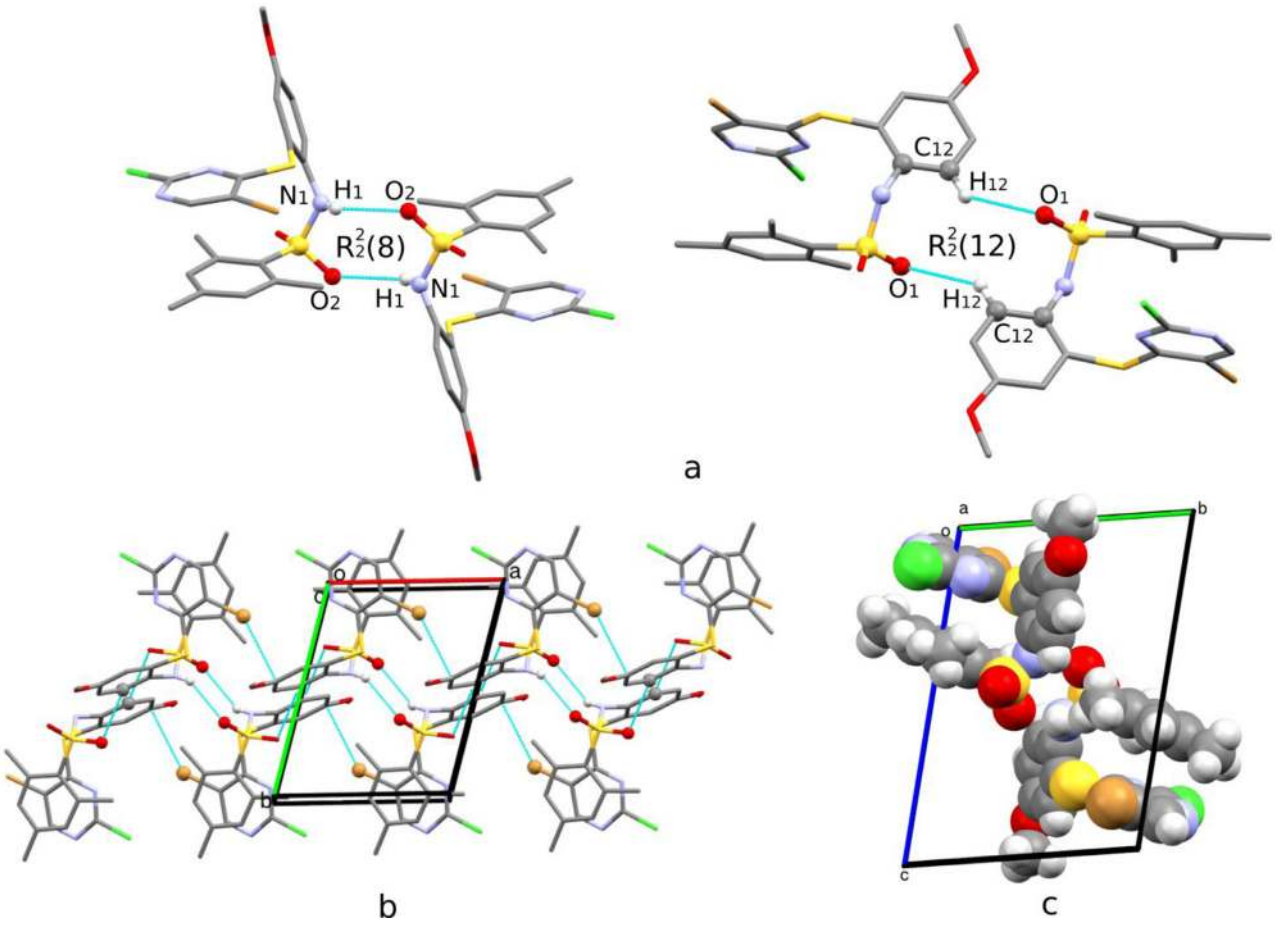

Fig. 2. (a) supramolecular $R_2^2(8)$ and $R_2^2(12)$ ring motif due to N1-H1N…O2 andC18-H18A…O2 inter molecular hydrogen bond interactions, (b) molecular packing along the ab-plane and (c) x-shaped one-dimensional array of molecules, lead to the formation of noncovalent Organic Framework along a-axis.

of the title compound are summarized in Tables S1, S2, and S3, respectively.

The crystal structure of benzene sulfonamide is quietly nonplanar and the molecule is preeminently twisted at sulfonamide moiety concerning methoxyphenyl and trimethyl rings with the interplanar angle of 52.24° and 65.15°, respectively (Fig. 1b). Chloro–bromo substituted pyrimidinyl ring is bridged by the sulfur atom (S2) with the methoxyphenyl ring in a non-planar manner with an interplanar angles of 75.31° (Fig. 1c). Trimethyl and chloro–bromo substituted pyrimidinyl rings are oriented face to face with the ring centroids distance of 3.530 Å leading to the weak intramolecular stacking interactions (Fig. 1d).

The molecular conformation ofbenzene sulfonamide is stabilized by various intermolecular interactions such as hydrogen bond interaction, C–H…Cg, C–H…Br/Cl… Cg and Cg…Cg interactions. N1-H1N…O2 and C18-H18A…O2 strong hydrogen bond interactions (Table 2 hydrogen bonds table) involved in the formation of $R_2^2(8)$ and $R_2^2(12)$ ring motifs (Fig. 2a), and these motifs are arranged adjacently in a zig-zag manner along c-axis(Fig. 2b), leading slanted x-shaped one-dimensional array of molecules along a-axis, where a smaller noncovalent molecular organic framework (MOF) can be observed throughout the crystallographic ab-plane (Fig. 2c). These molecular arrays are inter connected by the short Br…C10 [d(I-J): 3.327 Å] non-hydrogen intermolecular contacts which lead to the intermolecular clusters/networks.

Apart from intermolecular hydrogen bond interactions, C18-H18B…Cg3 *[H18B-Cg: 2.95 Å, C18-Cg3: 3.720(8) Å, C18-H18B…Cg3: 138.00° and symmetry code: x,1 + y, z]* and C14-Br…Cg3 *[Br-Cg3: 3.714(3) Å, C14-Cg3: 5.457(7) Å, C14-Br…Cg3: 154.05(18)° and symmetry code: −1 + x, y, z where Cg3 is the centroid of the chloro–bromo substituted pyrimidinyl ring]* intermolecular contacts exceedingly contribute to the crystal structure stability of benzenesulfonamide (Fig. 3a). Intermolecular $\pi\ldots\pi$ interactions between the centroids of methoxyphenyl and trimethyl rings [Cg-Cg: 3.529(4) Å], adjacent methoxyphenyl rings [Cg-Cg: 3.623(4) Å] and neighboring trimethyl rings [Cg-Cg: 4.512(4) Å (Fig. 3b)] are also eminently involved in the molecular packing of benzenesulfonamide (Table 3).

3.2. Hirshfeld surface (HS) analysis

The concept of HS is developed to specify the space occupied by a molecule in a crystal to divide the electron density of the crystal into molecular fragments of electron densities. A HS investigation is an effective tool to quantify the nature of intermolecular interactions present in the compound. The HS computations were carried out based on the crystallographic information file (CIF) using CrystalExplorer 17.5 software [35]. Fig. 4(a) shows the HS plotted over a normalized contact distance d_{norm}in the range from −0.3208 to 1.4202 a.u (overall volume = 529.64 Å). The mapping of d_{norm} onto the HS uses a red, white, and blue color scheme, where red, white, and blue spots show intermolecular contacts with distances less than, equal to, greater than van der Waal radii, respectively. The bright red region on the HS is due to C–H…O and N–H…O inter-

Table 2
X-H...π [X = C] and Y-X...π [Y = C, X=Br, Cl] interaction involved in the molecular structure.

X...H	Cg(J)	H...Cg (Å)	$H_{\perp}$ (Å)	γ (°)	X-H...Cg (°)	X...Cg (Å)	X-H...π (°)
C18-H18B	$Cg(3)^{i}$	2.95	−2.89	11.91	138	3.720(8)	49
X = C; i = x, 1 + y, z; Cg(3): C7-C8-C9-C10-C11-C12							
Y...X	Cg(J)	X...Cg (Å)	$X_{\perp}$ (Å)	γ (°)	Y-X...Cg (°)	Y...Cg (Å)	Y-X...π(°)
C14-Br	Cg(3)	3.714	3.298	27.38	154.05 (18)	5.457(7)	47.68
C16-Cl	Cg(1)	3.892	3.493	26.18	61.43 (19)	3.421(6)	2.39
[Y = C, X=Br,Cl] *i=−1 + x, y, z; ii = 2-x, 2-y, 2-z; Cg(3): C7-C8-C9-C10-C11-C12, Cg(1): N2-C13-C14-C15-N3-C16*							

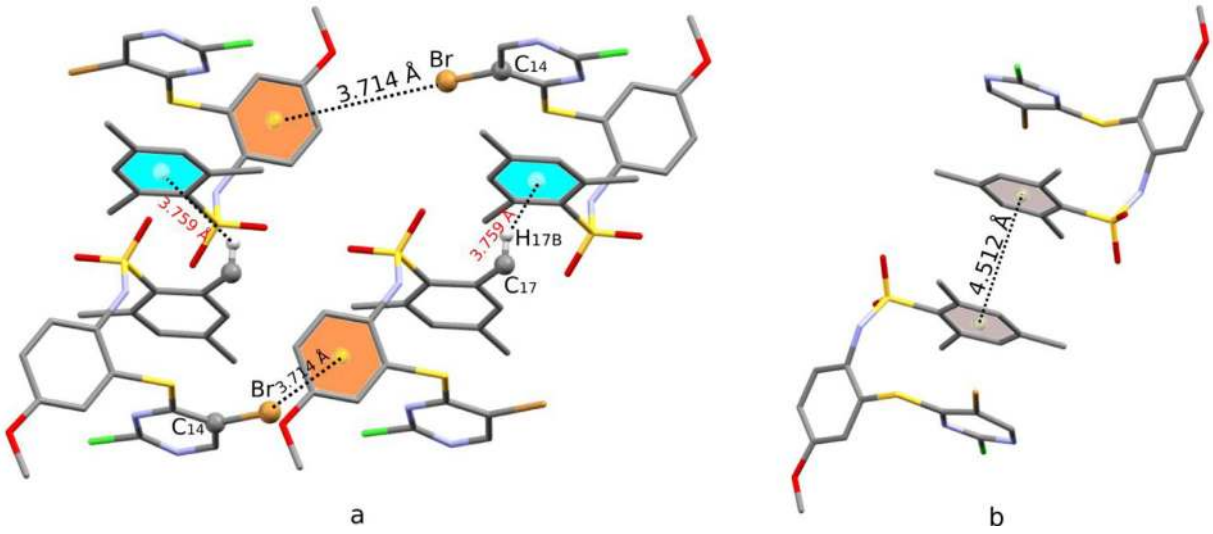

Fig. 3. (a) Intermolecular C–H...Cg, C-Br...Cg and (b) Cg...Cg interactions between the adjacent molecules of benzene-sulfonamide crystal.

Table 3
Cg-Cg interactions of the title molecule.

Cg(I)	Cg(J)	Cg-Cg	α	β	γ	$Cg(I)_{\perp}$	$Cg(J)_{\perp}$	Symmetry code
Cg(1)	Cg(1)	3.623(4)	0	20.5	20.5	3.394(2)	3.394(2)	*2-x, 2-y, 2-z*
Cg(1)	Cg(2)	3.529(4)	5.3(3)	15.0	17.3	3.369(2)	−3.410(2)	*x, y, z*
Cg(1)	Cg(3)	5.918(4)	74.4(3)	58.8	63.4	2.650(2)	3.069(2)	*2-x, 2-y, 2-z*
Cg(2)	Cg(3)	5.600(4)	69.8(3)	48.5	59.1	2.873	3.714(2)	*x, y, z*
Cg(3)	Cg(2)	5.556(4)	69.8(3)	18.4	80.5	−0.916(2)	−5.271(2)	*X, −1 + y, z*
Cg(1): N2-C13-C14-C15-N3-C16; Cg(2): C1-C2-C3-C4-C5-C6; Cg(3): C7-C8-C9-C10-C11-C12								

molecular contacts. The shape index surface for the title molecule consists of blue bumps and red dip (highlighted in the Fig. 4(b)) shows halogen (supports the C14-Br...cg3 and C16-Cl...cg1 interactions) and weak $\pi...\pi$ stacking interactions (triangle shaped region). Curvedness is a function of the root mean square curvature of the surface. The dark blue edges onto the curvedness surface are associated with intermolecular contacts (Fig. 4(b)) [36].

Further, two-dimensional fingerprint (FP) plots are employed to furnish quantitative information related to the nature and kind of intermolecular contacts occurred by the molecules in the crystal packing [37]. These 2D FP plots are investigated for each interatomic contact and overall interactions. In the computation of individual interatomic contacts, the reciprocal contact of each interatomic contacts is also included. Fig. 5(a) shows the 2D FP plot for overall interactions. The two spikes represent the interatomic contacts that have a significant contribution to crystal packing. The d_i and d_e are the distance from the HS to the nearest nucleus inside and outside the HS, respectively. The interatomic contacts that have a major contribution to crystal packing are H...H (38.0%), O...H (16.9%), C...H (10.3%), H...Cl (6.6%), and H...Br (5.1%).

The interaction of all the atoms presents inside the HS to an atom present in the vicinity of the HS is investigated and shown in Fig. 5(b). This investigation deduced that all the HS contained atoms interact strongly with the H atoms located in the region of the HS, and the percentage contribution of the ALL-H interaction is found to be 65.4%. Other such kinds of interactions are ALL-O, ALL-C, ALL-Br, ALL-Cl, ALL-N, ALL-S with contributions of 9.3, 9.2, 5.4, 5.3, 3.8, and 1.6%. These interactions are important to understand the crystal packing.

3.3. Interaction energy and 3D energy framework

Interaction energy and 3D energy framework analysis were carried out by using CrystalExplorer 17.5 software with the help of a crystallographic information file. This analysis was used for understanding the nature of interaction energies between molecu-

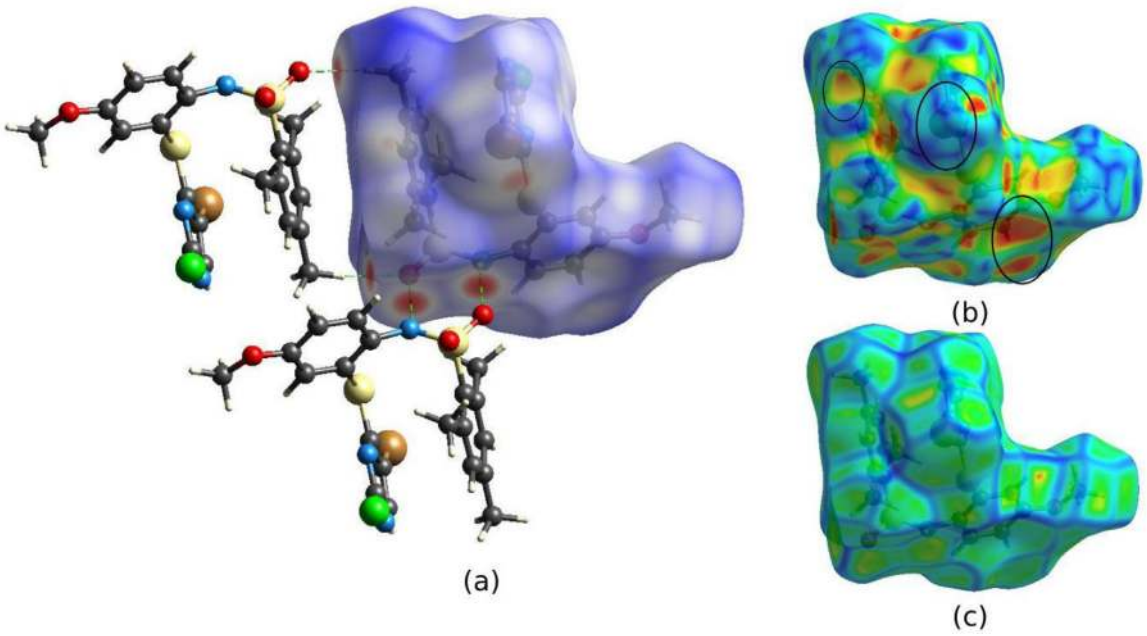

Fig. 4. HS plotted over (a) d_{norm}, (b) shape index, and (c) curvedness.

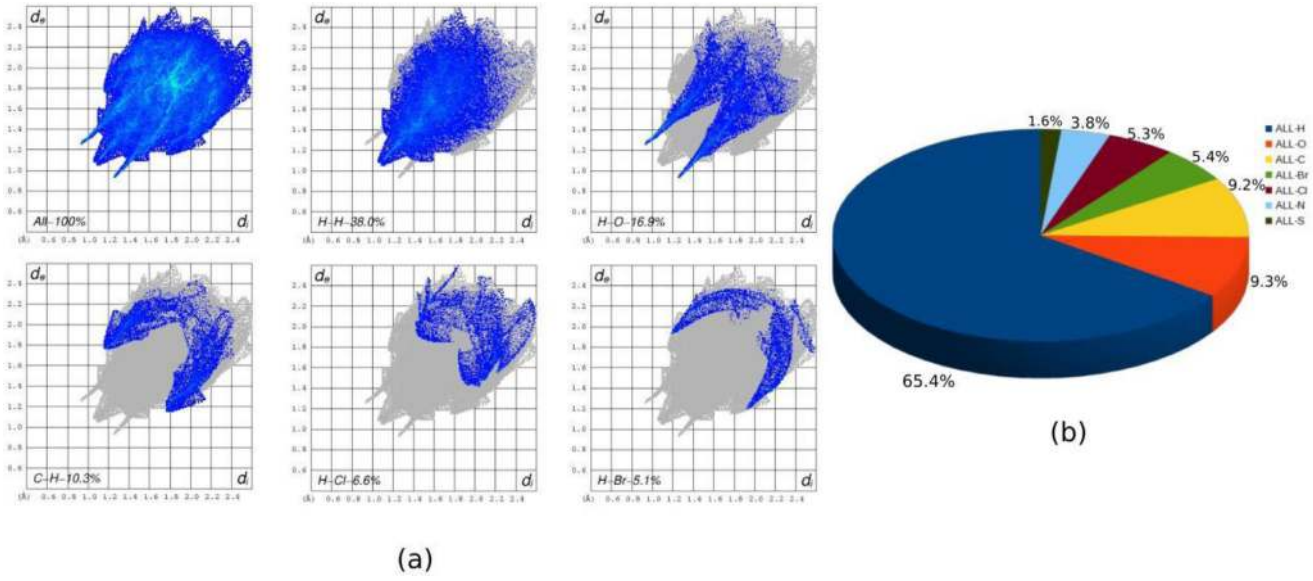

Fig. 5. (a) 2D FP plot for overall interactions and individual interactions in crystal packing of the title molecule (b) Percentage contributions of the interaction of all the atoms present inside the HS to an atom outside the HS.

lar pairs with a 3D graphical representation [38]. The interaction energies for the title molecule were computed by generating the cluster radius of 3.8 Å around the selected molecule and the results are summarized in Table 4. The total energies of the molecule were obtained by the sum of electrostatic (E_ele), dispersion (E_disp), polarization (E_pol), and repulsion (E_rep) energies. The molecular cluster with tube color represents the different types of energy profiles of the intermolecular interaction energies as shown in Fig. 6. Calculated total interaction energies of the title compound are electrostatic (−8.441 kcal/mol), dispersion (−15.468 kcal/mol), polarization (−2.548 kcal/mol), and repulsion (5.771 kcal/mol). The combination of these energies provides the total energy (−20.686 kcal/mol). Among these individual energies of the title molecule, dispersion energy is dominant over the electrostatic and polarization energies in the crystal environment.

3.4. DFT analysis

3.4.1. Molecular geometry

The electronic structure of the title compound is optimized by DFT/WB97XD level of theory with 6–311G(d,p) basis set [39]. The optimized bond lengths, bond angles, and dihedral angles of the title compound are summarized in Tables S1, S2, and S3, respectively. The optimized geometrical parameters are in good correlation with experimental data (crystal structure) obtained from the X-ray diffraction study. The overlay of the experimental and theoretical structure yields rmsd value of 2.09 Å for the title compound

Table 4
Molecular interaction energies (kcal/mol) of the cluster of molecules.

	N	Symmetry operations	*R* in Å	*E_ele*	*E_pol*	*E_dis*	*E_rep*	*E_tot*
	1	-x, -y, -z	8.56	-13.62	-4.400	-8.910	6.290	-19.670
	2	x, y, z	8.05	-1.36	-0.860	-11.329	6.501	-6.883
	1	-x, -y, -z	9.30	-6.31	-2.629	-8.963	5.473	-11.783
	1	-x, -y, -z	10.49	-4.88	-2.199	-5.019	2.414	-8.963
	2	x, y, z	9.91	-0.45	-0.406	-7.218	2.749	-4.995
	1	-x, -y, -z	10.81	0	-0.621	-5.043	3.107	-2.438
	1	-x, -y, -z	9.54	-1.22	-0.789	-5.330	1.362	-5.473
	1	-x, -y, -z	7.06	-3.56	-1.840	-16.850	8.700	-12.954
	1	-x, -y, -z	10.33	0.05	-0.263	-3.059	1.458	-1.697
	2	x, y, z	13.97	0.24	-0.048	-0.550	0.000	-0.287
	1	-x, -y, -z	14.89	-2.29	-0.359	-2.032	1.028	-3.561

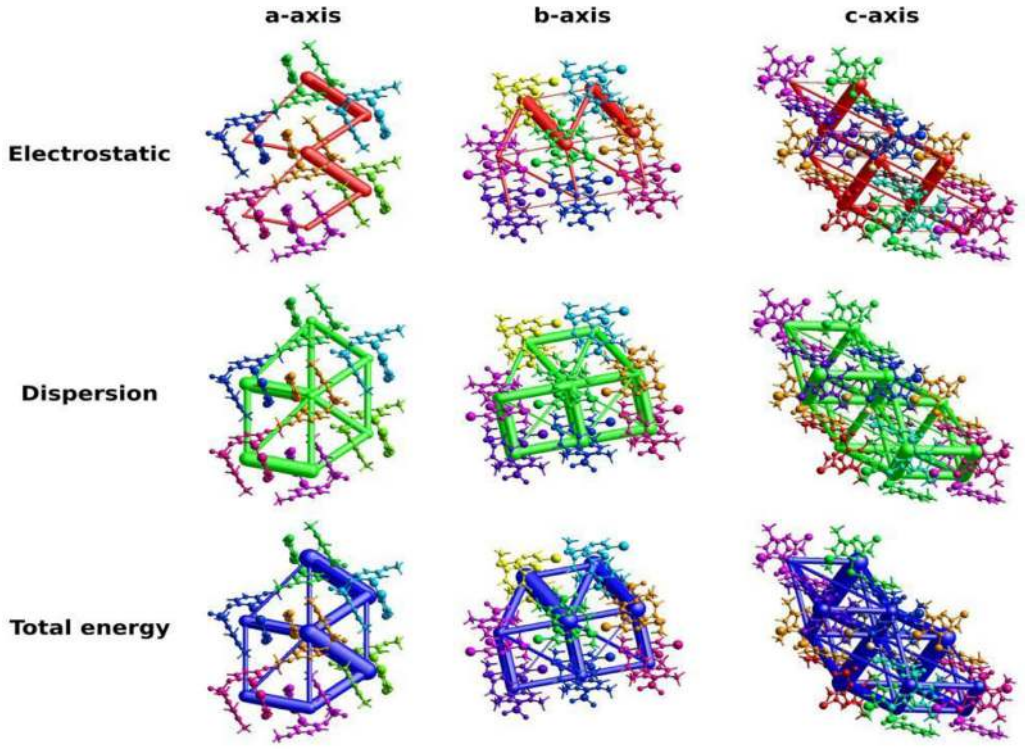

Fig. 6. The energy frameworks of the compound along *a, b, c*-axes for electrostatic energy, dispersion energy and total energy terms.

as shown in Fig. 7. Also, the comparison between experimental and calculated optimized structure parameters, bond lengths, bond angles, and torsion angles are tabulated in Tables S1, S2, and S3, respectively.

3.4.2. Frontier Molecular Oribitals (FMOs) and global reactivity parameters

FMOs containing the Highest Occupied Molecular Orbital (HOMO) which characterizes the ability of electron donating and Lowest Unoccupied Molecular Orbital (LUMO) which characterizes the ability of electron accepting as well as the energy gap were considered as effective parameters in chemical quantum chemistry [40]. The detailed information on chemical reactivity was obtained by this electronic absorption correlated to the transition from the ground state to the first excited state, and it was mainly explained by one electron excitation from the HOMO to LUMO orbital [41]. The 3D molecular distributions were observed in HOMO → LUMO, HOMO-1 → LUMO+1, and HOMO-2 → LUMO+2 as shown in Fig. 8 The energy gap of the title molecule was found to be 4.156 eV. The electron density of the HOMO concentrated on 4 methoxyphenyl but had a small effect on other 2,4,6 trimethyl phenyl**.** The concentration of the LUMO was revealed at 5–bromo-2–chloro-4-

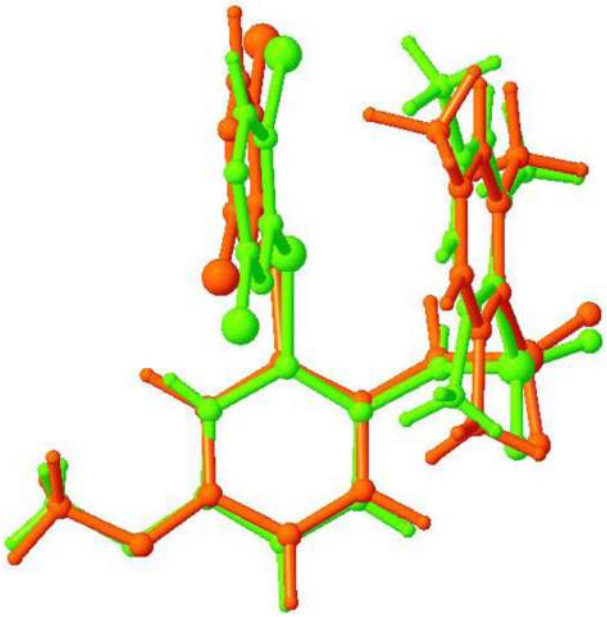

Fig. 7. Overlay of the crystal structure (green) and optimized electronic structure (orange) of the title compound.

pyrimidinyl. Also, the energy gap from HOMO-1 → LUMO+1, and HOMO-2 → LUMO+2 was determined as 4.9310 eV and 5.341 eV, respectively.

Total density of states (TDOS) represents the number of individual states at a specific energy level in which electrons are allowed to occupy. The TDOS in terms of Mulliken population analysis were calculated and created convoluting the molecular orbital information with Gaussian curves of unit height and full width at half maximum (FWHM) using *GaussSum 2.2* program. In this report, the TDOS plot of the title compound is plotted and shown in Fig. S1 (supplementary file). It furnishes a pictorial representation of molecular orbital compositions and their contributions to chemical bonding. The green color represents the HOMO and the red color represents the LUMO.

The stability and reactivity of the title molecule were explained by the HOMO-LUMO energies. Using Koopman's theorem, chemical hardness (η) chemical softness (s), and electronegativity (χ) of the title molecule were investigated and the corresponding values of the global parameters were listed in Table 5 [42].

3.4.3. Natural bond orbital (NBO) analysis

NBO analysis were performed to explain the charge transfer or delocalization of charge due to the intramolecular interaction among bonds. It also furnishes a convenient basis for investigating charge transfer or conjugative interaction in molecular systems.

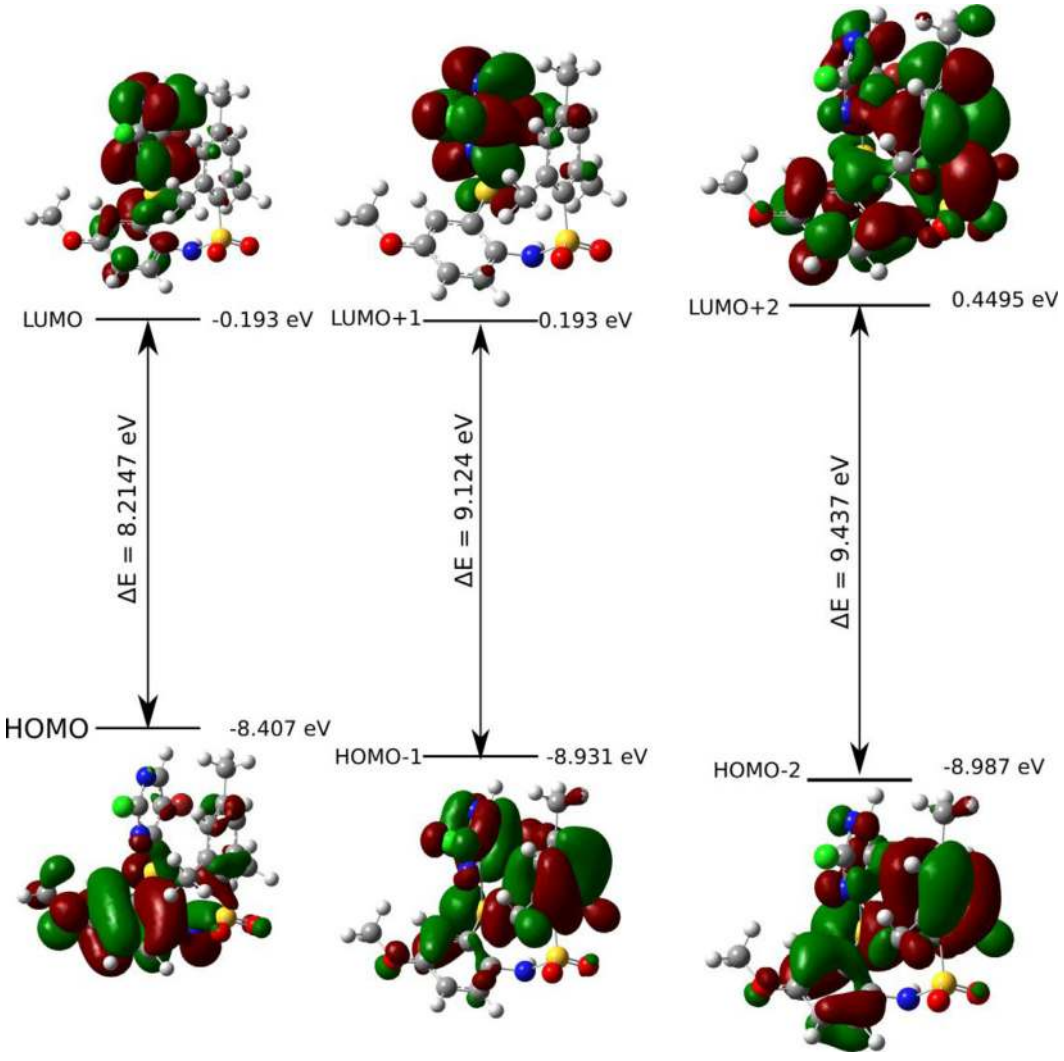

Fig. 8. Frontier molecular orbitals (FMOs) of the entitled compound.

Table 5
Calculated global reactivity parameters of the title compound.

Parameters	Values (eV)
Ionization potential (IP)	6.668
Electron affinity (EA)	2.512
Electronegativity (χ)	4.590
Chemical potential (μ)	−4.590
Global hardness (η)	2.078
Global softness (s) (eV-1)	0.481
Electrophilicity index (ω)	5.069
Charge transfer (ΔNmax)	2.209
Nucleofugality (ΔEn)	7.580
Electrofugality (ΔEe)	11.736

The second-order Fock matrix was carried out to investigate the donor–acceptor interactions in NBO analysis [43]. The interactions result is the loss of occupancy from the localized NBO of the idealized Lewis structure into an empty non-Lewis orbital. For each donor *(i)* and acceptor *(j)*, the stabilization energy $E^{(2)}$ associated with the delocalization $i \rightarrow j$ is estimated as

$$E^{(2)} = \Delta E_y = q_i \frac{F^{(2)}(ij)}{\varepsilon_j - \varepsilon_i}$$

where q_i is the donor orbital occupancy. ε_j and ε_i are diagonal elements and *F(i,j)* is the off diagonal NBO fock matrix element. Some of the electron donor orbital, acceptor orbitals (overlap) on which interacting stabilization energy $E^{(2)}$ resulting from the second order micro distribution theory. The larger the stabilization energy value, the stronger is the interaction between electron donors and electron acceptors. Delocalization of electron density between occupied Lewis type (bond or lone pair) NBO orbitals, and unoccupied (antibond or Rydberg) non-Lewis NBO orbitals correspond to a stabilizing donor-acceptor interaction. The stabilization energy or interaction energy ($E^{(2)}$) values for the filled (donor) and unfilled (acceptor) Lewis type NBOs are summarized in Table 6. It can be seen from Table 6 that the hyperconjugative interactions of the π-electrons from C–C bonding orbitals to the C–C anti-bonding orbitals stabilized the ring. In the title molecule, the electron delocalization from π^* (C9-C10) $\rightarrow$ π^* (C11-C12) has the highest stabilization energy $E^{(2)}$ = 330.64 kcal/mol. Besides, bonding and antibonding of C–C presented in the molecule may lead to stabilization of the ring. In addition, the π^*-π^*, LP-π^*, LP-σ^* and other interactions are also accountable for conjugation π-bonds and these interactions are involved in the maximum stabilization of the molecular systems.

3.4.4. Charge transfer due to excitation

The HOMO-LUMO gap gives rise to the charge transfer within the molecule. A correlation between HOMO-LUMO gap and charge transfer is obtained by studying the charge transfer within the molecule due to excitation. Multiwfn software is used to visualize the charge transfer due to the excitation for the first three excited states. The time dependent DFT (TD-DFT) calculations were made on the title compound using CAM-B3LYP/6–311G(d,p) as the basis set. The electron-hole (green-blue) distribution throughout the title compound for the 3 excited states is shown in Fig. 9. The integral of overlap of hole-electron distribution (S) is a measure of spatial separation of hole and electron, lesser the overlap more is the charge transfer. In order to investigate the existence and magnitude of the σ-hole at the Br atom, authors have performed the hole-electron excitation analysis. The hole-electron excitation analysis revealed the contribution of each atom to hole and electron. Br atom contributes to hole at the first, second and third excited state were found to be also, figure AA depicts the hole- electron distribution over the molecule in three excited states.

3.4.5. Molecular electrostatic potential (MEP) analysis

The chemical and physical aspects of any chemical system were investigated with the aid of MEP plot. The MEP plot was employed to comprehend the plausible reactive sites like electrophilic or nucleophillic sites present in the molecule. The MEP plot was calculated at DFT/WB97XD/6–311G(d,p) level. An electron isosurface mapped with electrostatic potential surface predicts the size, shape, charge density, and reactive sites of the molecule. The generated MEP plot of the title molecule is shown in Fig. 10. The MEP surface consists of standard colors like red, green, and blue. The order of magnitude of in the increasing order was found to be red < green < blue. The region highlighted with the red color was engaged to display the negative potential value related to electrophilic attack [44]. On the other side, the nucleophillic enticing site by the most positive potential value displayed with blue color, as shown in Fig. 10. From the figure, one can observe that, the negative region appears around the oxygen atom which is connected to the sulfur atom and the positive region is observed around the nucleophillic hydrogen atoms. The calculated results reveal that the overall surface area of the title molecule is 1503.452 Å^2, which consists of 887.651 Å^2 positive surface area and 615.801 Å^2 negative surface area. According to theoretical studies of halogen bonding, the outermost portion of the halogen surface has a region of positive electrostatic potential, and this positive region has been called the σ-hole. Also, the strength of the halogen bonding is correlated with the magnitude of V_{max} (positive electrostatic potential at the σ-hole) [45]. MEP map of the title compound with isosurface value of 0.002 shows the presence of σ-hole on the Br and Cl atoms (Fig. 10a and b). On these maps, the σ-hole is clearly indicated by the positive ESP on the X (X = Br, Cl) atoms in the axis of the C-X bond. One can notice that the blue color is more pronounced on the Br atom than on Cl atom. This suggest that the σ-hole on Br atom is deeper than the Cl atom. Magnitude of the σ-hole is examined by the topology of the MEP revealed that ESP maximum of 42 kcal/mol next to the Br hole and 17 kcal/mol near the Cl hole. With the formation of C-Br…π interaction, it is clear that the electronic charge transfers away from the halogen atom (Br).

3.4.6. Bader's quantum theory of atoms in molecules (QTAIM) and noncovalent interaction (NCI) index analyses

Noncovalent interactions like halogen and hydrogen bonds, C–H…π, π- π stacking interactions, and electrostatic and London dispersion forces [46] are predominantly important in chemistry and biochemistry. These interactions play a vital role in the title molecule, so it was important to shed a light on the non-covalent interactions. The various non-covalent interactions were identified and investigated via Bader's QTAIM analysis. Bader's QTAIM is a powerful method for determining the strengths and nature of non-covalent interactions at the electronic level based on topological parameters at bond critical points (BCPs). A BCP is a position where the gradient of electron density vanishes and is distinguished by one positive and two negative eigenvalues ($\lambda_1 < 0$, $\lambda_2 < 0$, $\lambda_3 > 0$) of the Hessian matrix. In this QTAIM analysis, different types of bonding interactions are qualitatively described by the ratio $|\lambda_1|/\lambda_3$ at the BCP. $\lambda_1|/\lambda_3 > 1$, electron density is mainly focused between atoms, leading to the covalent bond. Contrarily, when $\lambda_1|/\lambda_3 < 1$, electron density is concentrated around atoms, leading to non-covalent interactions like ionic, van der Waals, H-bonding interactions. Also, the electron density $\rho(r)$ and its Laplacian $\nabla^2\rho(r)$ at the BCP are key factors when characterizing bonding interactions. Large $\rho(r)$ values (greater than 0.20 a.u) and $\nabla^2\rho(r) < 0$ signify the polar and non polar covalent bonding interactions, whereas small $\rho(r)$ values (less than 0.10 a.u) and $\nabla^2\rho(r) > 0$ indicate non-covalent interactions. Koch and Popelier proposed the criteria for the existence of an H bond [47]:

Table 6
Second order perturbation theory analysis of Fock matrix in NBO basis for the title compound.

Donor (i)	Occupancy	Acceptor (j)	Occupancy	E(2) (kcal/mol)	E(j)-E(i)	F(i,j)
π*C9-C10	0.359	π*C11-C12	0.293	330.640	0.010	0.094
π*C7-C 8	0.433	π*C9-C10	0.359	204.440	0.020	0.100
π*C3-C 4	0.409	π*C1-C2	0.328	174.600	0.030	0.110
π*C3-C4	0.409	π*C5-C6	0.315	158.290	0.030	0.100
π*C7-C8	0.433	π*C11-C12	0.293	139.390	0.030	0.100
π*C16-N3	0.416	π*C14-C15	0.302	138.070	0.030	0.100
π*C13-N2	0.447	π*C14-C15	0.302	98.910	0.040	0.090
πC13-N2	1.715	π*C16-N3	0.416	52.890	0.420	0.140
πC14-C15	1.665	π*C13-N2	0.447	49.690	0.370	0.120
πC1-C2	1.639	π*C3-C4	0.409	47.530	0.370	0.120
πC16-N3	1.734	π*C14-C15	0.302	44.180	0.460	0.130
LP(O3)	1.841	π*C9-C10	0.359	42.180	0.470	0.130
πC5-C6	1.654	π*C1-C2	0.328	39.910	0.400	0.110

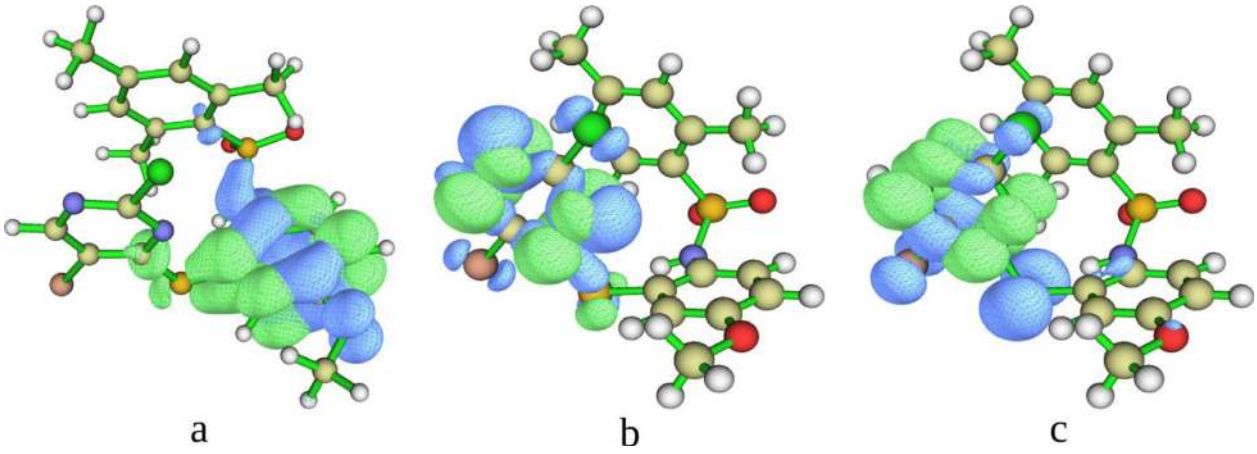

Fig. 9. Electron – hole distribution for the three excited states of the title compound.

Table 7
Topological parameters (in a.u) and hydrogen bond energies (kcal/mol) calculated on the WB97XD/6–311G(d,p) wave functions for the title compound.

Interactions	BCP	ρ_{BCP} (a.u.)	$\nabla^2\rho$ (a.u.)	V(r) (a.u.)	G(r) (a.u.)	$\frac{-G(r)}{V(r)}$	λ1	λ2	λ3	$\frac{\lvert\lambda_1\rvert}{\lambda_3}$	E_{HB} (kcal/mol)
C17-H…N2	57	0.00799	0.0257	−0.00438	0.0054	1.232	−0.0060	−0.0039	0.0357	0.168	−5.749
C14-Br…π	105	0.00442	0.0140	−0.00200	0.002756	1.1378	−0.0024	−0.0022	0.0187	0.1284	−2.625
π…π	82	0.00842	0.0238	−0.00397	0.00497	1.1251	−0.0043	−0.0022	0.0304	0.141	−5.2116
π…π	68	0.00939	0.0304	−0.00512	−0.00636	1.242	−0.0056	−0.0015	0.0376	0.148	−6.721
C17-H…S2	100	0.00705	0.0205	−0.00336	0.00424	1.261	−0.0032	−0.0019	0.0257	0.124	−4.410
C…S	111	0.0054	0.0177	−0.00261	0.00352	1.348	−0.0033	−0.0023	0.0233	0.141	−3.426
H…H	120	0.00704	0.0234	−0.00395	0.00491	1.258	−0.0057	−0.0040	0.0332	0.171	−5.185
C18-H…Cl	63	0.00484	0.0156	−0.00227	0.00309	1.361	−0.0032	−0.0030	0.0220	0.145	−2.979
C18-H…π	98	0.00831	0.0239	−0.0040	0.00503	1.257	−0.0061	−0.0027	0.0328	0.182	−5.251
C19-H…O3	127	0.0148	0.0567	−0.0108	0.0124	1.148	−0.0120	−0.0069	0.0757	0.158	−14.177

1 It must be accompanied by a BCP.
2 The ρ(r) value should fall within 0.002–0.040 a.u.
3 $\nabla^2\rho$(r) must be positive and should lie within 0.024–0.139 a.u.

In the present report, the values of $\nabla^2\rho$(r) and the ration -*G(r)/V(r)* were also used to characterize the bonding interactions involved in the title molecule (*G(r)*- kinetic energy density at the BCP, *V(r)*-potential energy at the BCP). When $\nabla^2\rho$(r) > 0 and ratio -*G(r)/V(r)*> 1, the interactions are non-covalent, whereas when $\nabla^2\rho$(r) >0 and 0.5 <-*G(r)/V(r)*<1, the interactions are partially covalent. The results from QTAIM analysis of the title compound are summarized in Table 7, and the corresponding BCPs with molecule is shown in Fig. 11(a). For this title molecule the Poincaré-Hopf relationship was satisfied, showing that all critical points have been found. The interatomic interaction energies (E_{int}) for the title molecule were estimated using the equation mentioned below,

$$E_{HB} = \frac{1}{2}V(r_{BCP})$$

One can observed from the Table 7 that all of the bonding interactions present in the title molecule are non-covalent in nature, since their ρ(r) values are less than 0.10 a.u. Also, the respective $\nabla 2\rho$(r) values are all positive and lie within the range 0.0140–0.0567 a.u. Further, the ratio $\frac{-G(r)}{V(r)}$ for all of these interactions at their BCPs are greater than unity, which is indicative of a non-covalent interactions and further validated by the fact that $\frac{|\lambda_1|}{\lambda_3} < 1$ in all cases ($\frac{|\lambda_1|}{\lambda_3}$values ranges from 0.124 to 0.182). The Eint values tells that the presence of weak and medium hydrogen bonds in the molecule. The interaction C19-H…O1 at the BCP 127 shows Eint as −14.177 kcal/mol which indicative of strong hydro-

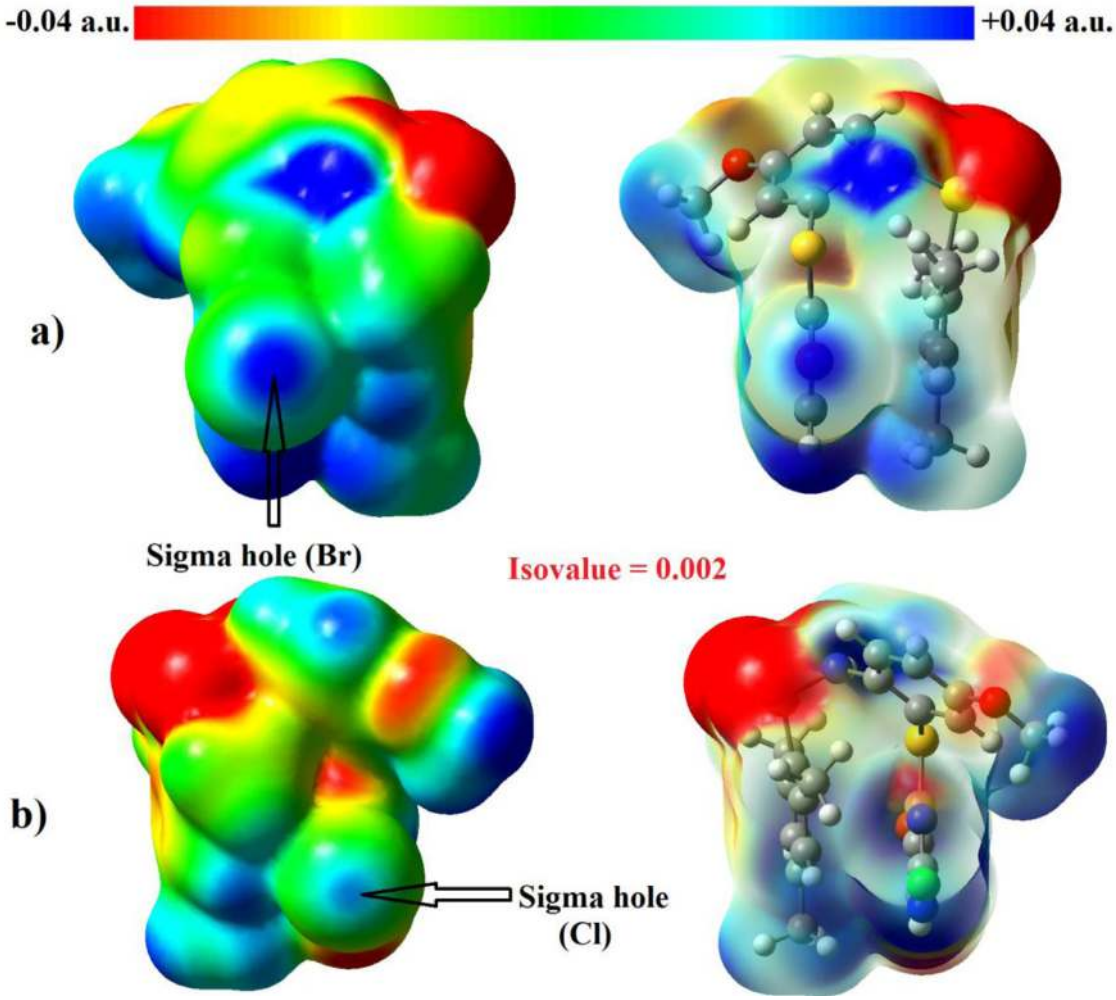

Fig. 10. MEP plot of the title compound.

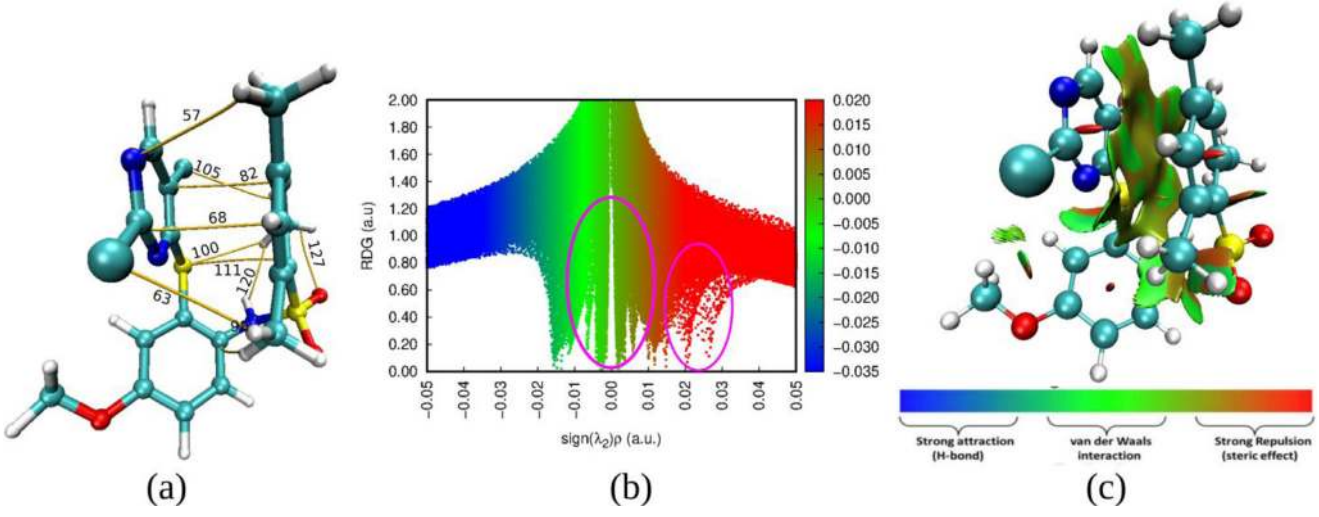

Fig. 11. (a) BCPs generated for the title molecule using QTAIM analysis (b) 2D scattered plot of the RDG vs *sign* (λ_2) and (c) non-covalent interactions (NCI) isosurface of electron density for the title compound.

gen bond interaction. Apart from the interaction C19-H…O1, the non-covalent interactions in the title molecule are very weak and appear to be dominated by van der Waals forces, as nearly all of the Eint values for these interactions are less than those of typical H-bonds.A detailed description of the attractive and repulsive non-covalent interactions in the molecular systems is crucial for understanding their functionality. The QTAIM analysis is based only on critical points in the electron density, but it excludes some weak non-covalent interactions. To overcome this problem, The NCI index is employed because it is based on the reduced density gradient (RDG), which is a function of the electron density ρ(r) and its first derivative $\nabla\rho$(r),

$$RDG(r) = \frac{\Delta\rho(r)}{2\left(3\pi^2\right)^{1/3}\rho(r)^{4/3}}$$

Using plots of RDG vs $\rho(r)$, the NCI index can be efficiently applied to identify the regions with non-covalent interactions as RDG tends to zero at low densities [48]. The NCI index uses the sign(λ_2) of the electron density Hessian matrix (λ_2) to distinguish between attractive ($\lambda_2 < 0$) and repulsive ($\lambda_2 > 0$). Interestingly, a two-dimensional scatter plot of RDG vs sign(λ_2) multiplied by the electron density $\rho(r)$ effectively splits the attractive regions from repulsive non-covalent interactions. Further, when sign(λ_2)$\rho(r)$ mapped onto a three-dimensional RDG isosurface, both the nature of non-covalent interactions and their strengths are highlighted using color coding; blue color is used for attractive interactions viz., H-bonds and halogen bonds, green colored region for very weak interactions such as van der Waals forces, red color for repulsive interactions (steric clashes) (Fig. 11(c)). The 2D NCI scatter plots of RDG against sign(λ_2)$\rho(r)$ for the title molecule is shown in Fig. 11(b), and this scattered plots furnishes the clear fingerprints of the non-covalent interactions involved in the title molecule.

The spikes present in the 2D scattered plot are related with the interaction of critical points (ICP). The strength of a non-covalent interaction is obtained from the electron density value corresponding to its ICP. A large negative value of the electron density indicates a stronger attractive ($\lambda_2 < 0$) or positive value of the electron density ($\lambda_2 > 0$) repulsive non-covalent interactions. The peaks at the low density region (sign(λ_2)$\rho(r) \simeq$ −0.015–0.015 a.u) in the scattered plots are indicative of the presence of van der Waals interactions. These van der Waals interactions are appeared as a big isosurface in the region between 5–bromo-2–chloro-4-pyrimidinyl and 2,4,6-trimethyl phenyl group. The larger positive value ((sign(λ_2)$\rho(r) \simeq$ 0.015–0.0 3a.u)) of the electron density indicates a stronger repulsion or steric clashes present in the phenyl rings of the title compound.

The BCP (132) was generated between C-Br and π-system (Fig. 12). The topological parameters corresponding to the BCP (132) are listed in the below table. The positive values of ρ_{BCP}, $\nabla^2\rho$, G(r) and $\frac{-G(r)}{V(r)}$ for the interaction is indicated the closed shell nature of the interaction. The ratio $\frac{-G(r)}{V(r)}$ for this interaction is greater than unity which is indicative of non-covalent interactions. Also, Independent gradient model (IGM) method is employed to calculate the inter fragment interactions using pro-molecular density. The green colored isosurface shows the weak interaction between the C-Br and…π system.

Interaction	BCP	ρ_{BCP} (a.u.)	$\nabla^2\rho$ (a.u.)	V(r) (a.u.)	G(r) (a.u.)	$\frac{-G(r)}{V(r)}$	λ_1	λ_2	λ_3	$\frac{\lvert\lambda_1\rvert}{\lambda_3}$
C-Br… π	132	0.0103	0.0342	−0.00561	0.00708	1.262	−0.0095	−0.0089	0.05277	5.547

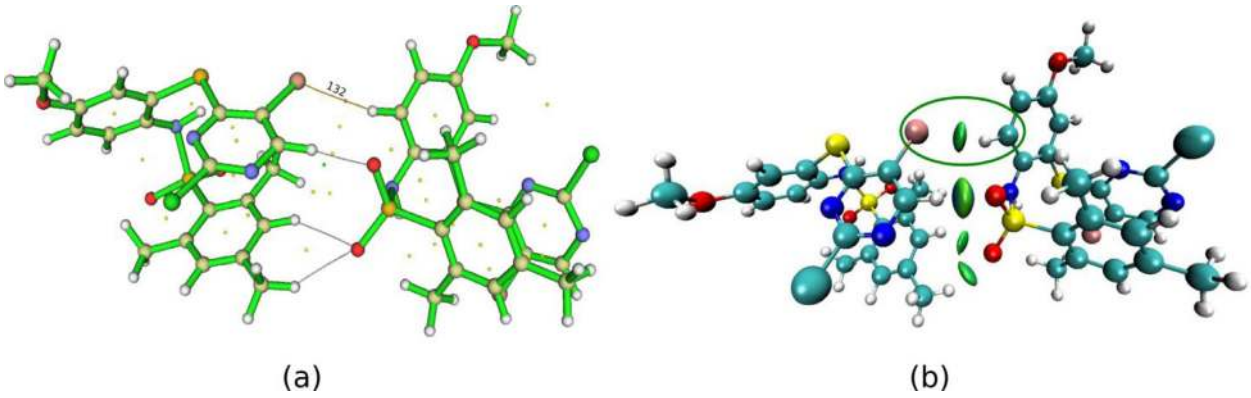

Fig. 12. (a) BCP generated for the C-Br…π interaction in the title molecule using QTAIM analysis (b) colored isosurface of C-Br…π interaction corresponding to IGM analysis.

4. Conclusion

A novel pyridine containing sulfonamide derivative was synthesized and its structure is confirmed by the SXRD analysis. H-bonding of the types N–H...O and C–H…O results in the packing of the molecules. HS analysis revealed that the H–H interatomic, whose contribution to the crystal packing is the strongest with a percentage contribution of 38.0%. The energy framework analysis revealed that the dispersion energy dominates over any other interaction energies. It is observed that for the studied molecule, the supramolecular synthons are due to the hydrogen bonds, π–π stacking and the halogen interactions contributing towards the solid-state packing. The study reinforced that dispersion correction is essential for accurate description non-covalent interactions present in the molecule. The nature of the inter and intramolecular interactions has been studied using structural analysis. The same is substantiated using the DFT calculations and characterized by the NBO, QTAIM and NCI analysis. Good agreement of the geometrical parameters was observed between the theoretical (DFT) and XRD values. The electronic changes have been monitored through the HOMO–LUMO gap and other global reactive parameters. NBO analysis explained the eventual charge transfer interaction taking place within the molecule. MEP quantified the sites available for hydrogen bonding. Also, global reactivity parameters were determined to assess the information related with the stability and reactivity of the molecule. QTAIM analysis revealed the closed shell nature of the interactions and NCI analysis unveiled the presence of non-covalent interactions in the title molecule.

CCDC- 2,115,842 contains the supplementary crystallographic data for this paper. These data can be obtained free of charge via https://www.ccdc.cam.ac.uk/structures/, or by e-mailing data_request@ccdc.cam.ac.uk, or by contacting The Cambridge Crystallographic Data centre, 12 Union Road, Cambridge CB2 1EZ, UK; fax: +44(0)1223–336,033″.

Declaration of Competing Interest

The authors declare that they have no known competing financial interests or personal relationships that could have appeared to influence the work reported in this paper.

CRediT authorship contribution statement

T.N. Lohith: Methodology, Writing – original draft, Data curation. **M.K. Hema:** Methodology, Writing – original draft, Software, Data curation. **C.S. Karthik:** Conceptualization, Methodology, Validation, Supervision, Writing – review & editing. **S. Sandeep:** Data curation, Formal analysis, Methodology. **L. Mallesha:** Methodology, Writing – review & editing. **Norah Salem Alsaiari:** Formal analysis. **M.A. Sridhar:** Data curation, Formal analysis, Methodology, Supervision, Writing – review & editing. **Khadijah M. Katubi:** Formal analysis. **Khamael M. Abualnaja:** Formal analysis. **N.K. Lokanath:** Validation. **P. Mallu:** Validation, Supervision. **S.R. Kumaraswamy:** Writing – review & editing.

Acknowledgment

Authors are thankful to SJCE, JSSSTU for providing computing facilities. This research was funded by Princess Nourah bint Abdulrahman University Researchers Supporting Project Number (PNURSP2022R19), Princess Nourah bint Abdulrahman University, Riyadh, Saudi Arabia. Also the author Dr Abualnaja appreciated Taif University Researchers Supporting Project number (TURSP-2020/267), Taif University, Taif, Saudi Arabia.

Supplementary materials

Supplementary material associated with this article can be found, in the online version, at doi:10.1016/j.molstruc.2022.133378.

References

[1] A.J. Neel, M.J. Hilton, M.S. Sigman, F.D. Toste, Exploiting non-covalent π interactions for catalyst design, Nature 543 (7647) (2017) 637–646.
[2] M. Mori, L. Kovalenko, S. Lyonnais, D. Antaki, B.E. Torbett, M. Botta, G. Mirambeau, Y. Mély, Nucleocapsid protein: a desirable target for future therapies against HIV-1, Future HIV-1 Ther. 389 (2015) 53–92.
[3] L.J. Chen, H.B. Yang, Construction of stimuli-responsive functional materials via hierarchical self-assembly involving coordination interactions, Acc. Chem. Res. 51 (11) (2018) 2699–2710.
[4] L. Brammer, Developments in inorganic crystal engineering, Chem. Soc. Rev. 33 (8) (2004) 476–489.
[5] M. Saccone, L. Catalano, Halogen bonding beyond crystals in materials science, J. Phys. Chem. B 123 (44) (2019) 9281–9290.
[6] N. Blagden, M. de Matas, P.T. Gavan, P. York, Crystal engineering of active pharmaceutical ingredients to improve solubility and dissolution rates, Adv. Drug Deliv. Rev. 59 (7) (2007) 617–630.
[7] S. Aitipamula, V.R. Vangala, X-ray crystallography and its role in understanding the physicochemical properties of pharmaceutical cocrystals, J. Indian Inst. Sci. 97 (2) (2017) 227–243.
[8] A. Kumar, A. Siwach, P. Verma, An overview of the synthetic route to the marketed formulations of pyrimidine: a review, Mini Rev. Med. Chem. 22(6) (2021) 884–903.
[9] Y. Yi, X. Xu, Y. Liu, S. Xu, X. Huang, J. Liang, R. Shang, Synthesis and antibacterial activities of novel pleuromutilin derivatives with a substituted pyrimidine moiety, Eur. J. Med. Chem. 126 (2017) 687–695.
[10] D. Giles, K. Roopa, F.R. Sheeba, P.M. Gurubasavarajaswamy, G. Divakar, T. Vidhya, Synthesis pharmacological evaluation and docking studies of pyrimidine derivatives, Eur. J. Med. Chem. 58 (2012) 478–484.
[11] A.M. Fargualy, N.S. Habib, K.A. Ismail, A.M. Hassan, M.T. Sarg, Synthesis, biological evaluation and molecular docking studies of some pyrimidine derivatives, Eur. J. Med. Chem. 66 (2013) 276–295.
[12] J. Xia, K. Zhang, E.A. Mahmood, Methods for the synthesis of N-aryl sulfonamides from nitroarenes: an overview, J. Sulfur Chem. 42 (6) (2021) 692–710.

[13] J. Boggavarapu, M. Nannapaneni, Synthesis and biological screening of pyrimidine linked benzene sulfonamide derivatives, International Journal of Pharmaceutical Science and Research 9 (12) (2018) 5534–5543.
[14] S. Mondal, S. Malakar, Synthesis of sulfonamide and their synthetic and therapeutic applications: recent advances, Tetrahedron 76 (48) (2020) 131662.
[15] P.K. Murthy, C. Valverde, V. Suneetha, S. Armaković, S.J. Armaković, N.U. Rani, N.V. Naidu, An analysis of structural and spectroscopic signatures, the reactivity study of synthetized 4, 6-dichloro-2-(methylsulfonyl) pyrimidine: a potential third-order nonlinear optical material, J. Mol. Struct. 1186 (2019) 263–275.
[16] R. Zeng, C. Lv, C. Wang, G. Zhao, Bionanomaterials based on protein self-assembly: design and applications in biotechnology, Biotechnol. Adv. 52 (2021) 107835.
[17] Z. Sharifzadeh, K. Berijani, A. Morsali, Chiral metal–organic frameworks based on asymmetric synthetic strategies and applications, Coord. Chem. Rev. 445 (2021) 214083.
[18] Z. Lu, S. Bai, Y. Shi, D. Xu, C. Chu, G. Liu, Artificial nanocage-based 3D framework platforms: from construction design to biomedical applications, Chem. Eng. J. 426 (2021) 131891.
[19] R.B. Lin, Y. He, P. Li, H. Wang, W. Zhou, B. Chen, Multifunctional porous hydrogen-bonded organic framework materials, Chem. Soc. Rev. 48 (5) (2019) 1362–1389.
[20] D.P. Devore, T.L. Ellington, K.L. Shuford, Interrogating the Interplay between Hydrogen and Halogen Bonding in Graphitic Carbon Nitride Building Blocks, J. Phys. Chem. A 124 (51) (2020) 10817–10825.
[21] M. Chahkandi, H.A.R. Aliabad, Crystalline network form of Gefitinib molecule stabilized by non–covalent interactions: DFT–D calculations, Chem. Phys. 525 (2019) 110418.
[22] C. Mallikarjunaswamy, L. Mallesha, D.G. Bhadregowda, O. Pinto, Studies on synthesis of pyrimidine derivatives and their antimicrobial activity, Arab. J. Chem. 10 (2017) S484–S490.
[23] Bruker APEX2 (Version 1.22) and SAINT-Plus (Version 7.06a), 2009.
[24] G.M. Sheldrick, A short history of SHELX, Acta Crystallogr. Sect. A Found. Crystallogr. 64 (2008) 112–122.
[25] G.M. Sheldrick, Crystal structure refinement with SHELXL, Acta Crystallogr., Sect. C: Struct. Chem. 71 (2015) 3–8.
[26] A.L. Spek, Single-crystal structure validation with the program PLATON, J. Appl. Crystallogr. 36 (2003) 7–13.
[27] C.F. Macrae, I. Sovago, S.J. Cottrell, P.T. Galek, P. McCabe, E. Pidcock, M. Platings, G.P. Shields, J.S. Stevens, M. Towler, Mercury 4.0: from visualization to analysis, design and prediction, J. Appl. Crystallogr. 53 (2020) 226.
[28] M. Frisch, G. Trucks, H. Schlegel, G. Scuseria, M. Robb, J. Cheesemana, V. Zakrzewski, J. Montgomery, R. Stratmann, J. Burant, Gaussian 98, Revision A. 11.4, Gaussian, Inc., Pittsburgh, PA, 2002 http://www.gaussian.com./.
[29] C.D. Duffy, A. Pandit, A.V. Ruban, Modeling the NMR signatures associated with the functional conformational switch in the major light-harvesting antenna of photosystem II in higher plants, Phys. Chem. Chem. Phys. 16 (12) (2014) 5571–5580.
[30] R. Dennington, T. Keith, J. Millam, GaussView, Version 5l, Semichem Inc., 2009.
[31] M. Rocha, A. Di Santo, J.M. Arias, D.M. Gil, A.B. Altabef, Ab-initio and DFT calculations on molecular structure, NBO, HOMO–LUMO study and a new vibrational analysis of 4-(dimethylamino) benzaldehyde, Spectrochim. Acta Part A Mol. Biomol. Spectrosc. 136 (2015) 635–643.
[32] T. Lu, F. Chen, Multiwfn: a multifunctional wavefunction analyzer, J. Comp. Chem. 33 (5) (2012) 580–592.
[33] W. Humphrey, A. Dalke, K. Schulten, VMD: visual molecular dynamics, J. Mol. Graph. 14 (1) (1996) 33–38.
[34] M.K. Priya, B.K. Revathi, V. Renuka, S. Sathya, P.S. Asirvatham, Molecular structure, spectroscopic (FT-IR, FT-Raman, 13C and 1H NMR) analysis, HOMO-LUMO energies, Mulliken, MEP and thermal properties of new chalcone derivative by DFT calculation, Mater. Today Proc. 8 (2019) 37–46.
[35] S. Yeşilbağ, E.B. Çınar, N. Dege, E. Ağar, E. Saif, Crystal structure and Hirshfeld surface analysis of dimethyl 3, 3′-{[(1E, 2E)-ethane-1, 2-diylidene] bis (azanylylidene)} bis (4-methylbenzoate), Acta Crystallogr. Sect. E Crystallogr. Commun. 78 (4) (2022) 340–345.
[36] M.K. Hema, R.R. ArunRenganathan, S. Nanjundaswamy, C.S. Karthik, Y.H.I. Mohammed, S. Alghamdi, P. Mallu, N-(4-bromobenzylidene)-2, 3-dihydrobenzo [b][1, 4] dioxin-6-amine: synthesis, crystal structure, docking and *in-vitro* inhibition of PLA2, J. Mol. Struct. 1218 (2020) 128441.
[37] S. Daoui, E.B. Çınar, N. Dege, N. Benchat, E. Saif, K. Karrouchi, Crystal structure of (E)-3-({6-[2-(4-chlorophenyl) ethenyl]-3-oxo-2, 3-dihydropyridazin-4-yl} methyl) pyridin-1-ium chloride dihydrate, Acta Crystallogr. Sect. E Crystallogr. Commun. 78 (4) (2022) 458–462.
[38] K.M. Chandini, F.H. Al-Ostoot, E.E. Shehata, N.Y. Elamin, H. Ferjani, M.A. Sridhar, N.K. Lokanath, Synthesis, crystal structure, Hirshfeld surface analysis, DFT calculations, 3D energy frameworks studies of Schiff base derivative 2, 2′-((1Z, 1′ Z)-(1, 2-phenylene bis (azanylylidene)) bis (methanylylidene)) diphenol, J. Mol. Struct. 1244 (2021) 130910.
[39] M.K. Hema, I. Warad, C.S. Karthik, A. Zarrouk, K. Kumara, K.J. Pampa, N.K. Lokanath, XRD/DFT/HSA-interactions in Cu (II) Cl/phen/ß-diketonato complex: physicochemical, solvatochromism, thermal and DNA-binding analysis, J. Mol. Struct. 1210 (2020) 128000 Struct. 2017, 1141, 142−156.
[40] Y. Oueslati, S. Kansız, N. Dege, C. de la Torre Paredes, A. Llopis-Lorente, R. Martínez-Máñez, W.S. Sta, Growth, crystal structure, Hirshfeld surface analysis, DFT studies, physicochemical characterization, and cytotoxicity assays of novel organic triphosphate, J. Mol. Model. 28 (3) (2022) 1–13.
[41] N. Dege, H. Gökce, O.E. Doğan, G. Alpaslan, T. Ağar, S. Muthu, Y. Sert, Quantum computational, Spectroscopic Investigations on N-(2-((2-chloro-4, 5-dicyanophenyl) amino) ethyl)-4-methylbenzenesulfonamide by DFT/TD-DFT with different solvents, molecular docking and drug-likeness researches, Colloids Surf. A Physicochem. Eng. Asp. 638 (2022) 128311.
[42] Arun Gurumallappa, R.R. Arun Renganathan, M.K. Hema, C.S. Karthik, S. Rani, M. Nethaji, H.S. Jayanth, P. Mallu, N.K. Lokanath, V. Ravishankar Rai, 4-acetamido-3-nitrobenzoic acid-structural, quantum chemical studies, ADMET and molecular docking studies of SARS-CoV2, J. Biomol. Struct. Dyn. 39 (2021) 1–15.
[43] T. Karthick, V. Balachandran, S. Perumal, A. Nataraj, Rotational isomers, vibrational assignments, HOMO–LUMO, NLO properties and molecular electrostatic potential surface of N-(2 bromoethyl) phthalimide, J. Mol. Struct. 1005 (1–3) (2011) 202–213.
[44] J. Chakkamalayath, K.R.S. Chandrakumar, S.K. Ghosh, Reactivity parameters and substitution effect in organic acids, J. Phys. Chem. A 124 (19) (2020) 3770–3777.
[45] Z. Chen, G. Wang, Z. Xu, J. Wang, Y. Yu, T. Cai, W. Zhu, How do distance and solvent affect halogen bonding involving negatively charged donors? J. Phys. Chem. B 120 (34) (2016) 8784–8793.
[46] V. Balachandran, T. Karthick, S. Perumal, A. Nataraj, Comparative theoretical studies on natural atomic orbitals, natural bond orbitals and simulated UV-visible spectra of N-(methyl) phthalimide and N-(2 bromoethyl) phthalimide, Indian Journal of Pure and Applied Physics 51 (3) (2013) 178–184.
[47] C. James, A. Amal Raj, R. Reghunathan, I.H. Joe, V.S. Jayakumar, Structural conformation and vibrational spectroscopic studies of 2,6-bis(*p*-*N*,*N*-dimethyl benzylidene)cyclohexanone using density functional theory, J. Raman Spectrosc. 37 (2006) 1381–1392.
[48] M. Szafran, A. Komasa, E.B. Adamska, Crystal and molecular structure of 4-carboxypiperidinium chloride (4-piperidinecarboxylic acid hydrochloride), J. Mol. Struct. Theochem. 827 (2007) 101–107.